Research Article

Melt electrowriting of poly(vinylidene fluoride-*co*-trifluoroethylene)

Juliane C Kade,[a] Biranche Tandon,[a,b] Jan Weichhold,[a] Dario Pisignano,[c,d] Luana Persano,[c] Robert Luxenhofer[e,f*] and Paul D Dalton[a,b*]

Abstract

Poly(vinylidene fluoride-*co*-trifluoroethylene) (P(VDF-co-TrFE)) is an electroactive polymer with growing interest for applications in biomedical materials and flexible electronics. In this study, a solvent-free additive manufacturing technique called melt electrowriting (MEW) has been utilized to fabricate well-defined microperiodic structures of the copolymer (P(VDF-co-TrFE)). MEW of the highly viscous polymer melt was initiated using a heated collector at temperatures above 120 °C and required remarkably slow collector speeds below 100 mm min^{-1}. The fiber surface morphology was affected by the collector speed and an increase in β-phase was observed for scaffolds compared to the unprocessed powder. Videography shows vibrations of the P(VDF-co-TrFE) jet previously unseen during MEW, probably due to repeated charge buildup and discharge. Furthermore, piezo-force microscopy measurements demonstrated the electromechanical response of MEW-fabricated fibers. This research therefore achieves the melt electrohydrodynamic processing of fibers with micrometer resolution into defined structures with an important electroactive polymer.

© 2021 The Authors. *Polymer International* published by John Wiley & Sons Ltd on behalf of Society of Industrial Chemistry.

Supporting information may be found in the online version of this article.

Keywords: additive manufacturing; electrohydrodynamic; electroactive; polymer processing

INTRODUCTION

Electroactive polymers with piezoelectric properties are of increasing interest for biomedical applications, in particular for the electrical stimulation of cells without the need for an external power supply.[1–4] Poly(vinylidene fluoride) (PVDF) and the copolymer poly(vinylidene fluoride-*co*-trifluoroethylene) (P(VDF-co-TrFE)) are often used for biomedical applications[2,5–9] owing to their flexibility, non-toxicity and good chemical resistance.[1,2,6,10] The piezoelectric properties of such polymers emerge when the crystalline structure is in the all-*trans* conformation which results in a net dipole moment.[1] PVDF is piezoelectric in the β-phase conformation, the content of which can be increased at the expense of the α-phase (*trans-gauche-trans-gauche* conformation) by stretching, poling or annealing of the raw material.[9,11] In contrast, P(VDF-co-TrFE) inherently prefers to crystallize into a crystal structure similar to the all-*trans* conformation (β-phase) due to the steric hindrance provided by the higher amount of fluorine atoms introduced by TrFE.[1,12–14] However, to improve the alignment of polymer chains/crystalline domains and generate a continuous macroscopic polarization, the copolymer P(VDF-co-TrFE) needs to be polarized by an electric field.[14]

Solution electrospun PVDF and P(VDF-co-TrFE) have been extensively studied for tissue engineering applications by Arinzeh and colleagues.[7,15–19] Small diameter P(VDF-co-TrFE) fibers (*ca* 970 ± 480 nm) showed *in vitro* cytocompatibility using human skin fibroblasts[19] and improved neurite extension using Schwann

cells and/or dorsal root ganglion[7,18] and human neural stem/progenitor cells.[17] An increase in chondrogenic and/or osteogenic differentiation of human mesenchymal stem cells on PVDF[16] and P(VDF-co-TrFE) fibers[15] has also been shown.

Due to the increasing interest in PVDF-based polymers, a variety of processing technologies have been studied in an attempt to increase the β-phase, as well as to investigate methods to control

* *Correspondence to: R Luxenhofer, Polymer Functional Materials, Department of Chemistry and Pharmacy, Julius-Maximilians-University Würzburg, Würzburg, 97070, Germany, E-mail: robert.luxenhofer@helsinki.fi; or PD Dalton, Department of Functional Materials in Medicine and Dentistry, Bavarian Polymer Institute, University Hospital Würzburg, Pleicherwall 2, Würzburg, 97070, Germany. E-mail: paul.dalton@fmz.uni-wuerzburg.de, pdalton@uoregon.edu*

a *Department of Functional Materials in Medicine and Dentistry, Bavarian Polymer Institute, University Hospital Würzburg, Würzburg, Germany*

b *Phil and Penny Knight Campus for Accelerating Scientific Impact, University of Oregon, Eugene, OR, USA*

c *NEST, Istituto Nanoscienze-CNR and Scuola Normale Superiore, Pisa, Italy*

d *Dipartimento di Fisica, Università di Pisa, Pisa, Italy*

e *Polymer Functional Materials, Department of Chemistry and Pharmacy, Julius-Maximilians-University Würzburg, Würzburg, Germany*

f *Soft Matter Chemistry, Department Chemistry, Helsinki Institute of Sustainability Science, Faculty of Science, University of Helsinki, Helsinki, Finland*

the fabrication of samples and constructs.[9] However, most of these processing methods involve use of toxic solvents; therefore, an alternative and solvent-free processing approach for fabricating fibers is via the melt. When accurate fiber placement is desired, one can utilize melt electrowriting (MEW) which gives excellent control over fiber placement. The enhanced control provided by MEW allows scaffolds to be directly written with defined structures and pore sizes.[20–24] Previously, a piezoelectric polymer (PVDF) was processed via MEW for the first time, with the fibers having increased β-phase content compared to the unprocessed powder.[25] To date, the copolymer P(VDF-co-TrFE) has been processed predominantly using solution electrospinning (SES) and film drawing. Both approaches require post-treatment to either remove toxic solvents, a particularly pertinent step for biomedical applications, or to maximize the macroscopic polarization (β-phase) by applying an electrical field.[14]

This study investigates the processing of P(VDF-co-TrFE) using MEW and determines the printability of the copolymer with this technique. The influence of the high viscosity of the material on the MEW process and the resulting scaffolds is investigated. Furthermore, a heated collector was essential with the temperature found to affect the overall crystallinity and β-phase content in the fibers. A collector temperature of 120 °C, close to the Curie temperature of the polymer when heating, was found to improve crystallization and consequently led to a higher amount of β-phase. Interestingly, buckling of the fibers occurred when the collector temperature was reduced to room temperature.

EXPERIMENTAL

Materials
P(VDF-co-TrFE) (Solvene® 200/P200; 80 mol% VDF, 20 mol% TrFE; #900895) was purchased from Sigma Aldrich (Taufkirchen, Germany) and used as received. The melt flow index, as provided by the manufacturer, is 25 g (10 min)$^{-1}$ (ASTM D1238).

Melt electrowriting (MEW)
The MEW processing of P(VDF-co-TrFE) was performed with a custom-built device as previously described,[26] which operated at a nitrogen (N$_2$) pressure of 0.5 bar. A stainless steel nozzle was attached to a 3 mL glass syringe (Fortuna Optima 3 mL Luer Lock). The flat-tipped nozzle was prepared by grinding an injection cannula (22 gauge with Luer Lock, Carl Roth, Germany) to a length of 7.0 $\pm$ 0.2 mm. The print head and nozzle tip temperatures were set to a value of 170 $\pm$ 2 °C as reported by respective thermocouples. A potential difference of $+3.70 \pm 0.20$ kV was applied between the nozzle and the grounded collector plate. MEW was maintained at a collector distance of 4.4 $\pm$ 0.5 mm, with 3.0 $\pm$ 0.2 mm of the nozzle protruding beyond the electrowriting head. A heated collector was custom-built as previously described[26] and set to 120–135 $\pm$ 5 °C during printing. Glass microscope slides (VWR, ground edge, cat # 631-1550) were chosen as a printing substrate and were placed on top of the heated collector. The glass syringe was loaded with approximately 0.5 g of P(VDF-co-TrFE) and pre-heated for at least 30 min prior to printing. MEW processing was conducted at collector speeds between 10 and 100 mm min^{-1}.

X-ray diffraction (XRD)
XRD spectra were collected using a Bruker D8 Advance. The operating voltage and current used were 30 kV and 53.3 mA. The samples were irradiated with Cu Kα radiation using a step size of

0.045°, a dwell time of 0.7 s and a rotation of 15 r in the 2θ range 10°–80° with a low background sample holder made of a specially cut silicon single crystal. The raw powder and MEW-processed scaffolds printed with speeds of 50, 70 and 100 mm min^{-1} at two different collector temperatures (120 and 135 °C) were measured by placing them directly on the sample holder without further fixation. Background corrections and calculations on the measurements were done using a beam knife and the software DIFFRAC.TOPAS.

Imaging and videography
Stereomicroscope images were taken with a Discovery V20 (Carl Zeiss Microscopy GmbH, Germany). SEM imaging of the MEW-processed fibers and scaffolds was performed with a Crossbeam 340 (Carl Zeiss Microscopy GmbH) instrument with all samples sputter-coated with approximately 3 nm of platinum (Leica EM ACE600). Videography was done using a Sony Alpha 7 and Nikon Z6 digital camera with Nikon ED 200 mm lens. Editing of the videos was performed using the software DaVinci Resolve 16.2.7.01.

Fiber diameter
A tabletop scanning electron microscope (TM3030p, Hitachi High-Tech Corporation) was used to take images from three different samples with four printed single lines per collection speed, which was varied between 10 and 100 mm min^{-1}. These images were then used to measure the diameter with ImageJ (Version 1.52a, National Institutes of Health, USA) at around 50 different locations for at least three samples per collection speed.

For the measurements of the top and bottom fibers, SEM images, of a scaffold with 10 layers in each direction, were taken at three different positions. Therefore, while imaging, the focus was set either on the bottom or the top layers and 15 different positions were measured within one image. In total three images of the bottom or top fibers were taken.

Atomic force microscopy (AFM) and piezo-force microscopy (PFM)
The morphological/electromechanical characterization of P(VDF-co-TrFE) fibers deposited onto indium tin oxide coated glass substrates at a collector speed of 90 mm min^{-1} and temperature of 120 °C was carried out by AFM and piezo-force microscopy (PFM). Measurements were done in contact mode by using a conductive diamond-coated probe with a nominal spring constant of 80 N m^{-1} (Bruker, USA) on a Bruker Dimension Icon system, equipped with a Nanoscope V controller. The surface roughness was calculated as the average of the root mean square values for areas of 25 μm^2 distributed along the fiber backbone.

RESULTS

Fiber fabrication
The processability of the P(VDF-co-TrFE) via MEW was initially tested using parameters traditionally used for this technology; however, extruding P(VDF-co-TrFE) proved to be difficult compared to other polymers. Owing to the high viscosity of the polymer (melt flow index 25 g (10 min)$^{-1}$, ASTM D1238), a pressure greater than 1 bar was tested for polymer extrusion and jet initiation. However, it was observed that the pressurized gas would sometimes push through within the nozzle, resulting in poor extrusion. Following jet stabilization at high pressures, the oscillating jet (Video S1, 0.25× original speed) became electrostatically

attracted towards the print head and led to jet breakup (Video S2, 1.5× original speed). Therefore, despite the high viscosity of the P(VDF-co-TrFE), a lower N_2 pressure of 0.5 ± 0.1 bar was selected for further experiments.

Further experiments revealed that, due to the rapid solidification of the polymer melt, the extruded material did not adhere to the collector and was dragged over the surface of the collector (Video S3), similar to what was previously observed for polypropylene.[26] This issue of jet dragging was solved using a collector heated to temperatures of 120–135 °C. P(VDF-co-TrFE) fibers were printed onto glass slides using two different collector temperatures. The resulting fibers were uniform and demonstrated good adherence to the collector substrate with the possibility to stack up to 20 alternating layers in 0°–90° orientation. Using SEM imaging for fiber morphology, it was revealed that fibrils are formed normal to the fiber orientation during the crystallization and solidification process of the polymer melt (Fig. 1). Similar results, showing extended grain growth and crystallization for SES fibers at annealing temperatures above 115 °C, were observed by Kim *et al.*[27] Melt electrospun polymers have also shown similar surface morphologies.[28]

Using a collector temperature of 135 °C, the fibers start to show partial fusion and flattening onto the collector surface, consequently losing their circular shape (Fig. 1(D)). Removing the printed fibers and scaffolds from the glass slides without damage was challenging for the higher collector temperature of 135 °C, as the scaffolds adhered more to the glass surface. A lower collector temperature of 120 °C results in uniform and stable fibers that can be processed without noticeable flattening and can be detached without difficulties. Therefore, the use of a heated collector adds another adjustable instrument parameter for MEW of polymers where jet initiation is an issue due to non-adherence (Video S3).

One of the notable outcomes of this study, in strong contrast to all other polymers processed to date using MEW, is the very low collector speed required for direct writing. Straight fibers, albeit with a larger 50 μm diameter, could be collected using collector speeds as low as 10 mm min^{-1} and it was difficult to determine a critical translation speed (CTS) where a transition between sinusoidal and linear deposition indicates the speed of the electrified jet.[24,29] Much higher CTS values were previously reported for other polymers including poly(ϵ-caprolactone) (300–750 mm min^{-1}),[24] urea-siloxane thermoplastic elastomers (1500–3500 mm min^{-1})[22] and poly(ϵ-caprolactone-*co*-acryloyl carbonate) (150–750 mm min^{-1}).[20] The lowest CTS value previously reported was for polypropylene (50–150 mm min^{-1}), which is also a polymer that requires a heated collector for direct writing.[26] This indicates that rapid cooling of the jet is probably responsible for the lack of a CTS in this instance. It was observed that above a maximum collector speed of approximately 100 mm min^{-1} the molten jet readily 'snapped' and continuous direct writing could not be achieved. Clearly, MEW processing parameters for P(VDF-co-TrFE) differ rather significantly from all previously processed materials.

Thermal analysis of raw polymer and scaffolds was performed to study the effect of high processing temperatures on P(VDF-co-TrFE). TGA revealed that the mass of the P(VDF-co-TrFE) melt remains constant over the measured period of 5 h at 170 °C to simulate the conditions during the MEW process (Fig. S1(A)). A color change of the melt from colorless/transparent to yellow-brown could be observed in line with that similarly observed for PVDF.[25] This color change may be attributed to low molar mass additives or unknown residues from the synthesis, rather than the polymer. At higher temperatures around 300 °C, TGA shows a significant reduction in the mass representing the onset of degradation of polymer. In the DSC measurements (Fig. S1(B)) both the polymer and the scaffolds showed the same peaks in the second heating cycle suggesting no change in the polymer due to MEW processing. The cooling curves from DSC (Fig. S1(B)) showed a Curie transition around approximately 75–80 °C for both powder and MEW scaffolds. This Curie transition is lower for the cooling of the P(VDF-co-TrFE) compared to the Curie transition measured upon heating (135 °C) of the polymer. At the Curie temperature a transition from the ferroelectric to paraelectric phase is taking place.[30,31]

Effect of collector speed on fiber diameter

To investigate the influence of the collector speed on the crystallization process and fiber diameter, it was varied from 10 to 100 mm min^{-1} in 10 mm min^{-1} increments at the aforementioned collector temperatures of 120 ± 5 °C and 135 ± 5 °C. The resulting fibers were imaged by SEM (Fig. 2). Increasing the collector speed results in a decrease of the fiber diameter for both
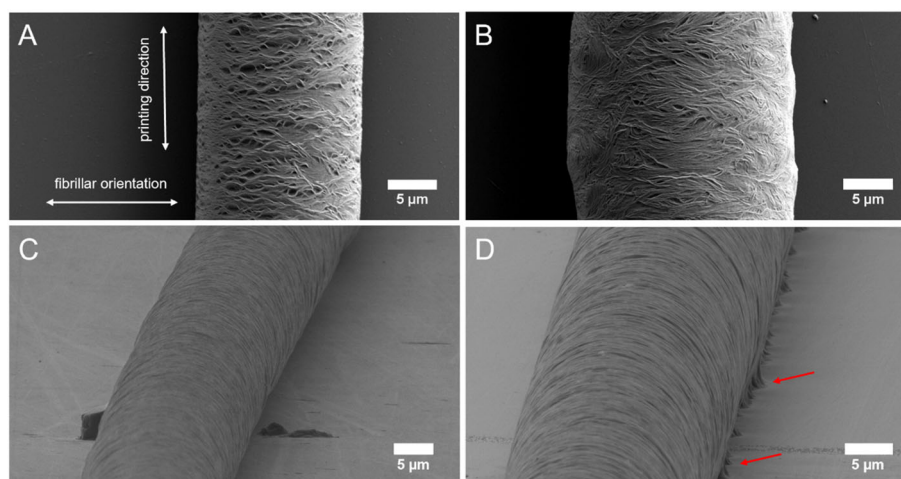
Figure 1. SEM images of fibers direct-written at 50 mm min^{-1} onto collectors heated at (A), (C) 120 °C and (B), (D) 135 °C. SEM images showing (A), (B) the top view of fibers depicting the printing direction and fibrillar orientation and (C), (D) the side view of the fibers. Fiber fusion and melting on the heated collector is highlighted by red arrows (D).

collector temperatures. Above 30 mm min^{-1}, the decrease in fiber diameter levels off at around 15 μm for both collector temperatures (Fig. S2(A)). A similar behavior has been described previously for polycaprolactone.[32]

SEM images also showed differences in the formation of crystalline domains with varying fiber diameters. The change in the fiber morphology depending on the collector speed can be attributed to changes in collector temperature and cooling behavior of the jet. A change in the fiber morphology depending on the annealing temperature has been reported in the literature.[27] The fiber morphology can be related to grain growth and crystallization[27] and might be explained by a phase transition from the α-phase into the piezoelectric, *all-trans zig-zag* β-phase. This phase transformation has been previously described by different groups[33–35] as a transformation from a spherulitic to a microfibrillar structure and can be induced by stretching of the molten jet. The radial spherulitic structure is visible on MEW fibers directly written with a collector speed of 10 mm min^{-1} (Figs 2(A), 2(D)) and transforms into different surface morphologies with increasing collector speed (Figs 2(B), 2(C), 2(E), 2(F) and in magnified view in Fig. 1). Those surface morphologies could be caused by the stretching of the jet into a fibrillar structure from crystallites.[33,35] Furthermore, the collector speed influenced the jet lag of the polymer melt[24,36] (Video S4; speed of the videos was adjusted to match the print duration of 10 mm min^{-1} prints) and might lead to different cooling rates of the printed fibers, which in turn influence the crystallinity of the fibers. As previously observed for MEW-processed fibers, changes in the surface morphology can also originate from disparities in the solidification rates of the fiber surface and core.[37] It is known that, with increasing collector speeds, the electrified jet is increasingly stretched.[24,36]

Layer stacking behavior

With the direct-writing parameters for single fibers established, the fabrication of multi-layered 0–90° scaffolds, at 500 μm hatch spacing, with up to 10 alternating layers was investigated. Notably, and never reported before for MEW, printing more than three stacked layers on top of each other resulted in the formation of sinusoidal structures in between the crossing points, when cooling the collector to room temperature after printing (Fig. 3). This phenomenon was studied for the two different collector temperatures, different collector speeds and scaffolds with 0–90° and 0–45° fiber orientation. The collector temperature while printing seems not to have any significant influence on the formation of sinusoidal fibers; only the collector temperature while cooling appears to impact this phenomenon (Video S5).

The sinusoidal formation starts to appear when the collector temperature reaches about 70–80 °C at the glass slide and 80–90 °C for the set temperature of the heated collector (Video S5) and therefore could be connected to the Curie transition temperature during cooling as judged from the DSC thermograms (Fig. S1(B)). These structural variations could be due to changes in the recrystallization process during solidification and residual thermal strain, which are known to be highly dependent on the cooling rate.[37] However, the first two to three layers always stay straight independent of the collector speed or the collector temperature, probably due to increased adherence to the collector and to the underlying layers (red arrows, Fig. 3(B)).

When measuring the fiber diameter of the top and bottom layers of the scaffold (Fig. S2(B)), no significant decrease or increase was observed. When inspecting the turns of the lines within the scaffolds (Figs 3(E), 3(F)), the jet lag is pulling the fibers at the turns inwards, as previously observed for radial structures printed using medical-grade polycaprolactone.[38] Therefore, the position of the fiber changes with the number of layers when the directing of writing is substantially changing.

Furthermore, fabricated P(VDF-co-TrFE) scaffolds with 20 alternating layers at 0° and 90° showed the solidified fiber breaking in between the scaffolds at various locations. The breakage of the fiber could be due to (i) the jet breaking or (ii) mechanical
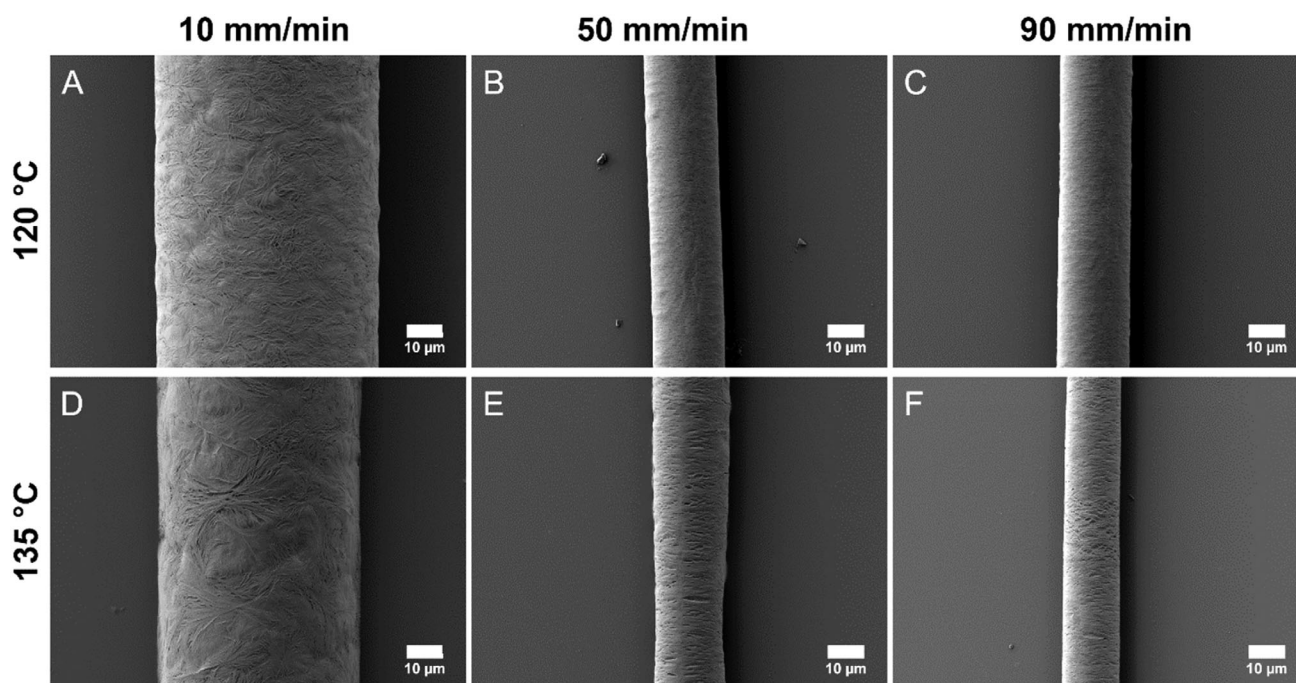
Figure 2. (A)–(F) SEM images of MEW-processed fibers printed at varying speeds (10, 50 and 90 mm min^{-1}) and two different collector temperatures (120 and 135 °C).
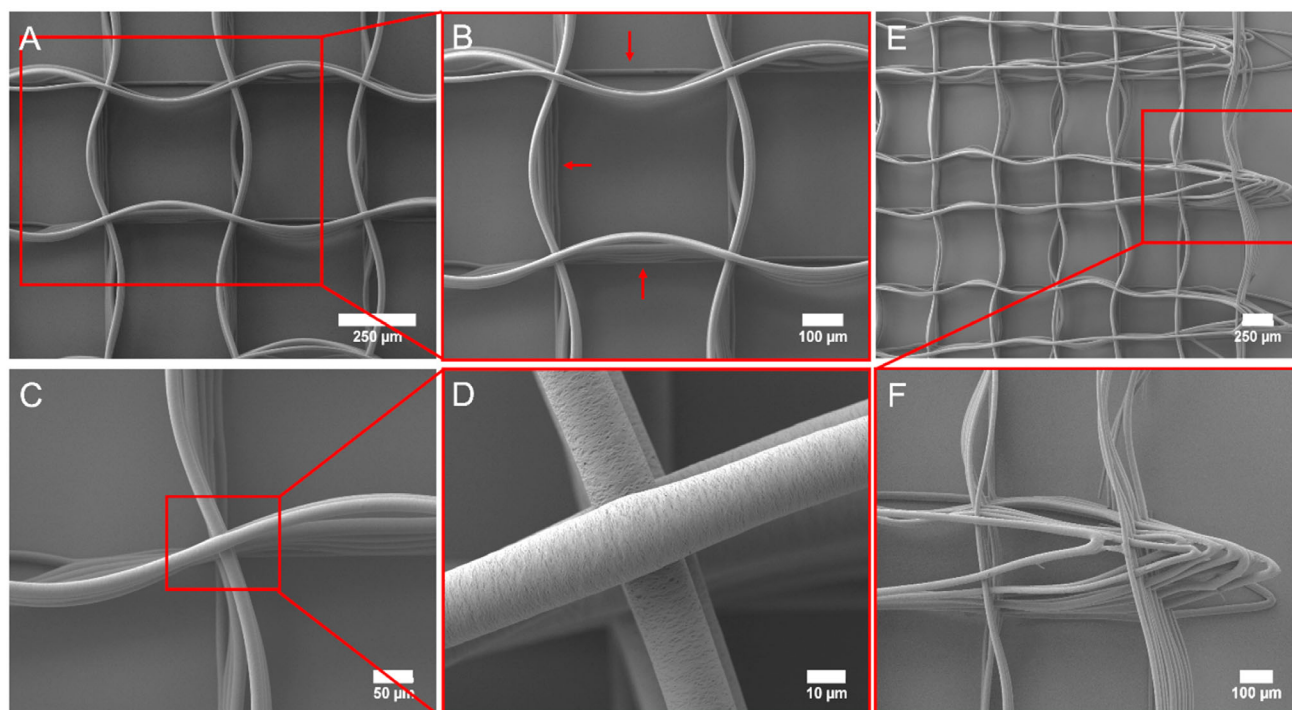
Figure 3. SEM images of a 0/90° scaffold: (A), (B) the box structure. Red arrows indicate the first three fibers deposited, which remain straight, unlike the sinusoidal nature of the higher layers. SEM images of (C), (D) the crossing points and (E), (F) the turns. (B), (C) and (F) show magnified views.
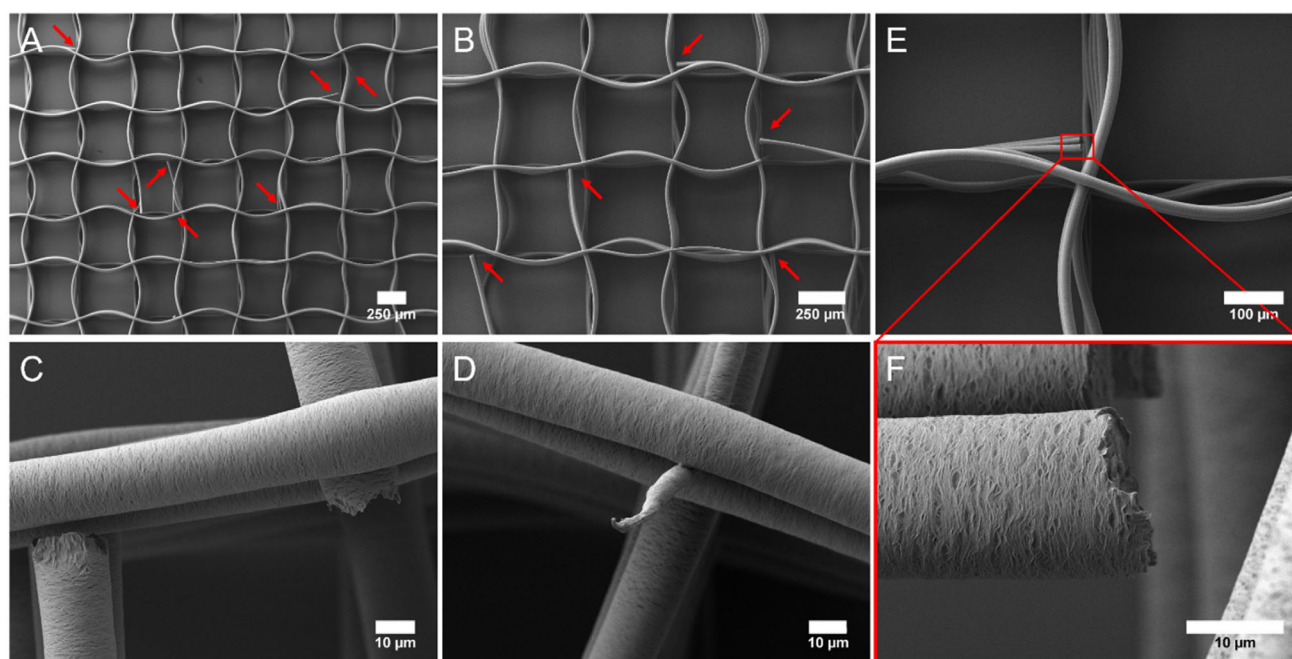
Figure 4. SEM images of 20 alternating layers with broken fibers and fiber bundle. (A), (B) Box structured scaffold with red arrows indicating brittle fractures. Magnified SEM images highlighting the differences between (C) a brittle fracture due to the bending/cooling crystallization process and (D) a snapped fiber caused by jet break-up. (E) Sharp breaks resulting in fiber bundles; (F) a magnified view.

forces associated with fiber bending while cooling. Figures 4(A) and 4(B) show an overview of a 20-layer P(VDF-co-TrFE) scaffold printed with a speed of 70 mm min^{-1} and a collector temperature of 120 °C. At various locations one or more fibers are snapped, indicated with red arrows (Figs 4(A), 4(B)); however, a clear trend

in where and when the fibers were breaking could not be determined. It seems that the fibers break probably due to rapid temperature changes, for example when removing the glass slides from the heated collector temperature (120–135 °C) to a surface at room temperature.

Another indication of fibers breaking post-solidification is that the broken fiber bundles remain at their position within the scaffold (Figs 4(C) and 4(E-F)). In comparison, the point of break within a jet break-up in the polymer melt is stretched and pulled until the jet snaps, resembling ductile failure behavior (Fig. 4(D)).

XRD measurements, crystallinity and β-phase content

The corresponding XRD measurements for the raw powder and the scaffolds printed at collector temperatures of 120 and 135 °C are displayed in Fig. 5. For the unprocessed P(VDF-co-TrFE) powder, a clearly visible shoulder peak can be seen at 18° and a peak at 20°, respectively, which can be attributed to the polar β-phase (110 and 200), as described previously for SES fibers.[6,27] For all MEW-processed scaffolds the shoulder peak at 18°, attributed to the α-phase, disappeared or reduced significantly. Comparing the measurements in Fig. 5(B), the peak at 20° is broader for the scaffolds printed with 50 and 70 mm min⁻¹. A similar broader peak can be seen at the collector temperature of 135 °C for the scaffold printed with 100 mm min⁻¹ (Fig. 5(C)). Therefore, MEW processing of the raw powder seems to decrease the α-phase, as previously observed for SES fibers due to the *in situ* poling and stretching while electrospinning.[6,15,27] However, as shown in Fig. 5(A), the intensity of the peaks is lower for the MEW-processed scaffolds compared to the unprocessed powder. For the scaffolds printed at 120 °C, the absolute intensity is lower compared to that of the unprocessed powder and higher compared to the scaffolds printed at 135 °C. Here, it needs to be mentioned that the XRD measurements were performed on MEW-fabricated scaffolds with high porosity compared to a filled up powder sample holder resulting in different intensities within the diffractogram measured for the samples.

From the XRD results, the ratio between α- and β-phase for the MEW-processed scaffolds printed at both collector temperatures can be calculated (Fig. S3 and Table S1). The background of the sample holder and crystalline phases within the XRD measurements of the unprocessed powder and MEW-fabricated scaffolds has been separated and the crystalline part was used for further investigations. Furthermore, the peaks of the crystalline region were separated into areas corresponding to the α- and β-phases as described in Fig. S3. A similar approach also using a multi-peaks fitting technique has previously been utilized based on DSC measurements.[39]

For both collector temperatures, the ratio between α- and β-phase content changed with β-phase contents at around 85% to 90% for the MEW-processed scaffolds. For the samples printed at the higher collector temperature with speeds of 50 and 70 mm min⁻¹ the β-phase content is around 90%; however, the total crystallinity is significantly less compared to the samples printed at a collector temperature of 120 °C (Table S1 and Fig. 5). Therefore, MEW processing of the P(VDF-co-TrFE) with a heated collector can be seen as an *in situ* annealing process and annealing temperatures close to the Curie temperature can provide sufficient energy for chain reorientation and therefore can lead to an increase in β-phase formation compared to unprocessed material.[27]

Using the set temperature and the actual measured collector temperatures, we were able to quantify the cooling rates with a slightly faster cooling rate for the 135 °C collector temperature. Therefore, the collector with the set temperature of 135 °C might lead to a decrease in crystallinity, as it is known that crystallinity is highly dependent on the cooling rate and a fast cooling rate can lead to a lower crystallinity.[40,41]

These β-phase contents are within the range of values shown in the literature for differently treated films resulting in β-phase fractions of 66.33% to 100% using P(VDF-co-TrFE) (75/25)[42] or P(VDF-co-TrFE) (80/20).[39] Furthermore, SES fibers result in values around 85% P(VDF-co-TrFE) (75/25) depending on the fiber orientation[6] and 88% β-phase using P(VDF-co-TrFE) (70/30).[43] Those findings together with the results of the MEW-processed fibers in this study indicate the high impact of the TrFE content, as well as the applied electric field, which is in general higher for SES and/or the fabrication process (melt- or solvent-based), on the resulting β-phase fractions and the overall crystallinity.

Jet behavior

Rapid cooling of the polymer was believed to be the reason for dragging of the polymer jet on the collector as discussed above. This issue was simply circumvented by using a heated collector. Another interesting phenomenon shown for the copolymer jet is the oscillating/vibrating behavior as depicted in Video S1. The balance between the amount of polymer and voltage applied was found to be the key to laying down fibers consistently for long durations. As the pressure was increased, the jet was readily attracted towards the head (Video S2) and disrupted the jetting process. The collector temperature of 120 °C and the applied
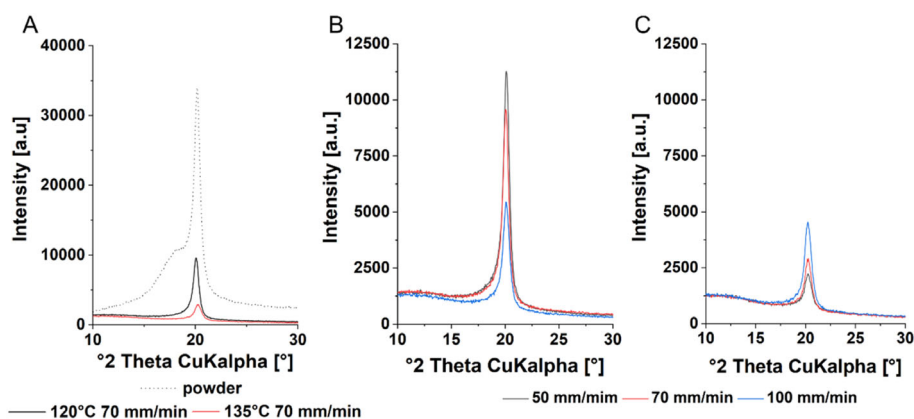
Figure 5. X-ray diffractogram showing (A) the raw P(VDF-co-TrFE) powder (dashed line) compared to scaffolds printed with 70 mm min⁻¹ at collector temperatures of 120 °C (black line) and 135 °C (red line). MEW scaffolds fabricated with speeds of 50 mm min⁻¹ (black line), 70 mm min⁻¹ (red line) and 100 mm min⁻¹ (blue line) at collector temperatures of (B) 120 °C and (C) 135 °C.
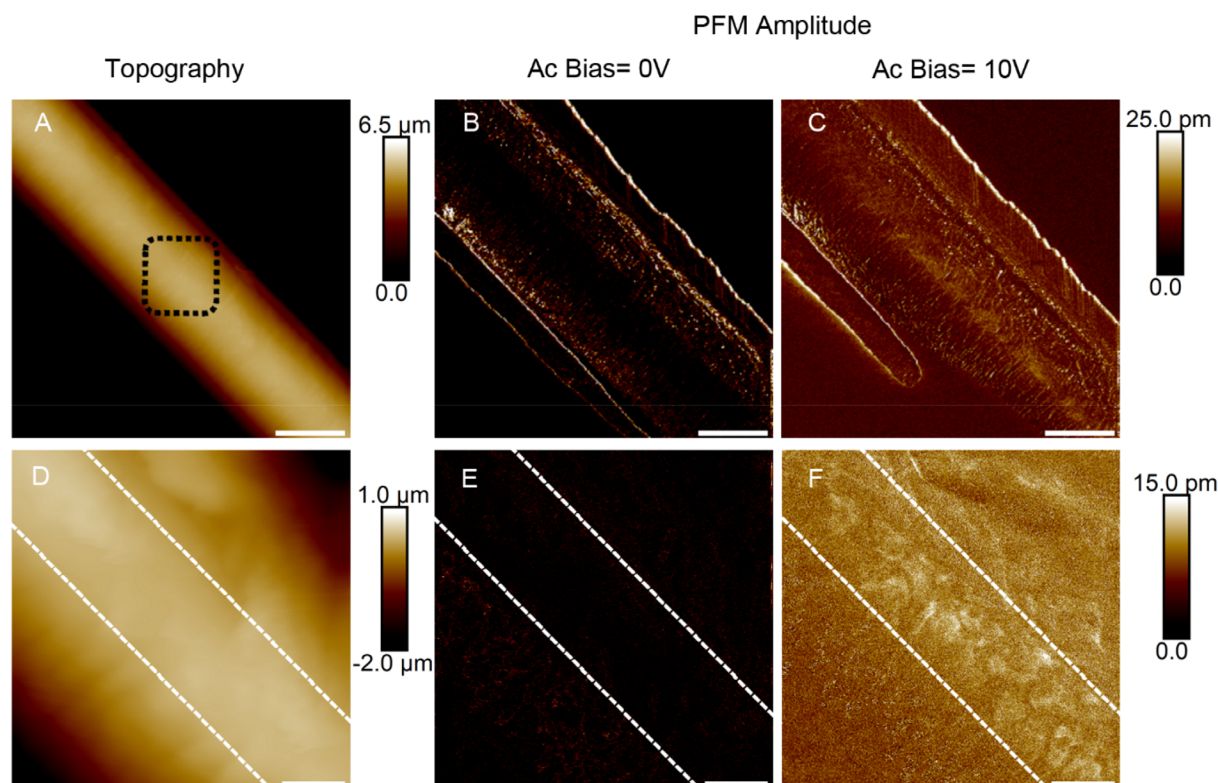
Figure 6. (A) AFM topographic images and corresponding PFM images of a P(VDF-co-TrFE) fiber at an AC bias voltage of (B) 0 V and (C) 10 V. (A)–(C) Scale bars 10 μm. (D)–(F) High magnification images of (A)–(C) measured in the area of the fiber highlighted by the black box in (A). The dashed white lines highlight the fiber backbone. (D)–(F) Scale bars 2 μm.

voltage were not sufficient to attract the jet and initiate the process of MEW.

The formation of a stable jet while printing is highly dependent on the processing parameters, especially the speed of the collector.[24,44,45] For other already established MEW-processable polymers, the CTS is a very important value and is sensitive to small changes in the processing parameters. The jet at speeds just above the CTS typically starts with a nearly vertical line and then increases the lag significantly until the lag seems to level off,[45] which can be related to the fiber diameter discussed previously. For the P(VDF-co-TrFE) a similar behavior was observed; however, no CTS was found and the processed fibers resulted in straight and uniform lines even at significantly low speeds of 10 mm min^{-1}. Looking at the jet lag of the P(VDF-co-TrFE), within the processable speed range from 10 to 100 mm min^{-1}, an increase in the jet lag depending on the collector speed was detected and the jet lag seems to level off at 50 mm min^{-1} and higher (Video S4).

Morphological and piezoelectric characterization

The piezoelectric response of the MEW-processed fiber was measured by PFM upon the application of an alternating (AC) voltage with a frequency of 15 kHz (Fig. 6). The measured fiber was deposited onto an indium tin oxide coated glass substrate at a collector speed of 90 mm min^{-1} and a temperature of 120 °C. The fiber diameter, taking into account a deconvolution of the profile of the AFM tip used, is 16 μm and the surface roughness along the fiber backbone is of the order of 100 nm. Upon the application of an AC bias of 10 V between the tip and the sample, the PFM amplitude signal indicates a strain response of tens of picometers, which is higher along the fiber backbone (Figs 6(C), 6(F))

highlighting a surface pattern that can be correlated with a local enhancement of the vertical component of the polarization vector in certain crystalline domains.

In contrast, the amplitude of the in-plane oscillation that was measured by lateral PFM indicates an almost uniform distribution of the in-plane piezo response (Fig. S4), suggesting different dynamics of crystallization and solidification along the fiber backbone. Changes in the PFM amplitude signal were measured for AC bias in the interval 2–10 V, leading to a linear dependence between the piezo response and the applied voltage typical of piezoelectricity (Fig. S5(A)). Dipoles are sensitive to the direction of the applied field and exhibit a phase shift when the external bias is inverted (i.e. the positive bias is applied to the sample and the tip is grounded) as reported in Figs S5(B) and S5(C).

CONCLUSION

In this study, an important piezoelectric polymer, P(VDF-co-TrFE), was shown to be processable via MEW into fibers ranging between 10 and 50 μm, depending on the collector speed. The direct writing had to be performed at remarkably low speeds of less than 100 mm min^{-1} while a heated collector was essential to initiate the direct writing. Upon cooling of the collector, straight fibers formed sinusoidal structures which were correlated to a change in the macromolecular orientation within the recrystallization process, in turn influenced by the collector temperature and speed. The resulting MEW-processed fibers showed a decrease in α-phase and an increase in the piezoelectric β-phase content of up to 85%–90% compared to the unprocessed powder even though the total crystallinity did not increase. The electroactive

nature of this polymer was proven by PFM measurements and makes this study relevant to applications where well-resolved 3D printed structures of such piezoelectric polymers are of interest, such as biomedical products due to the absence of toxic solvents compared to other processing techniques, as well as energy harvesting, actuators and sensors.

ACKNOWLEDGEMENTS

SUPPORTING INFORMATION

Supporting information may be found in the online version of this article.

REFERENCES

1 Rajabi AH, Jaffe M and Arinzeh TL, *Acta Biomater* **24**:12–23 (2015).
2 Zaszczynska A, Sajkiewicz P and Gradys A, *Polymers* **12**:161 (2020).
3 Palza H, Zapata PA and Angulo-Pineda C, *Materials* **12**:277 (2019).
4 Ribeiro C, Sencadas V, Correia DM and Lanceros-Méndez S, *Colloids Surf B Biointerfaces* **136**:46–55 (2015).
5 Liu X, Wang X, Zhao H and Du Y, *J Phys Conf Ser* **557**:012057 (2014).
6 Persano L, Dagdeviren C, Su Y, Zhang Y, Girardo S, Pisignano D *et al.*, *Nat Commun* **4**:1633 (2013).
7 Wu S, Chen M-S, Maurel P, Lee Y-s, Bunge MB and Arinzeh TL, *J Neural Eng* **15**:056010 (2018).
8 Zaarour B, Zhu L, Huang C and Jin X, *J Appl Polym Sci* **136**:47049 (2019).
9 Ribeiro C, Costa CM, Correia DM, Nunes-Pereira J, Oliveira J, Martins P *et al.*, *Nat Protoc* **13**:681–704 (2018).
10 Foster FS, Harasiewicz KA and Sherar MD, *IEEE Trans Ultrason Ferroelectr Freq Control* **47**:1363–1371 (2000).
11 Martins P, Lopes AC and Lanceros-Mendez S, *Prog Polym Sci* **39**:683–706 (2014).
12 Haque RI, Vié R, Germainy M, Valbin L, Benaben P and Boddaert X, *Flex Print Electron* **1**:015001 (2015).
13 Wan C and Bowen CR, *J Mater Chem A* **5**:3091–3128 (2017).
14 Hafner J, Teuschel M, Schneider M and Schmid U, *Polymer* **170**:1–6 (2019).
15 Damaraju SM, Shen Y, Elele E, Khusid B, Eshghinejad A, Li J *et al.*, *Biomaterials* **149**:51–62 (2017).
16 Damaraju SM, Wu S, Jaffe M and Arinzeh TL, *Biomed Mater* **8**:045007 (2013).
17 Lee Y-S and Arinzeh TL, *Tissue Eng Part A* **18**:2063–2072 (2012).
18 Lee Y-S, Collins G and Livingston Arinzeh T, *Acta Biomater* **7**:3877–3886 (2011).
19 Weber N, Lee YS, Shanmugasundaram S, Jaffe M and Arinzeh TL, *Acta Biomater* **6**:3550–3556 (2010).
20 Hochleitner G, Chen F, Blum C, Dalton PD, Amsden B and Groll J, *Acta Biomater* **72**:110–120 (2018).
21 Castilho M, van Mil A, Maher M, Metz CHG, Hochleitner G, Groll J *et al.*, *Adv Funct Mater* **28**:1803151 (2018).
22 Hochleitner G, Fürsattel E, Giesa R, Groll J, Schmidt H-W and Dalton PD, *Macromol Rapid Commun* **39**:1800055 (2018).
23 Hochleitner G, Jüngst T, Brown TD, Hahn K, Moseke C, Jakob F *et al.*, *Biofabrication* **7**:035002 (2015).
24 Hrynevich A, Elci BS, Haigh JN, McMaster R, Youssef A, Blum C *et al.*, *Small* **14**:e1800232 (2018).
25 Florczak S, Lorson T, Zheng T, Mrlik M, Hutmacher DW, Higgins MJ *et al.*, *Polym Int* **68**:735–745 (2019).
26 Haigh JN, Dargaville TR and Dalton PD, *Mater Sci Eng C* **77**:883–887 (2017).
27 Kim M, Lee S and Kim Y-i, *APL Mater* **8**:071109 (2020).
28 Dalton PD, Grafahrend D, Klinkhammer K, Klee D and Moller M, *Polymer* **48**:6823–6833 (2007).
29 Dalton PD, *Curr Opin Biomed Eng* **2**:49–57 (2017).
30 Meng N, Zhu X, Mao R, Reece MJ and Bilotti E, *J Mater Chem C* **5**:3296–3305 (2017).
31 Furukawa T, Johnson GE, Bair HE, Tajitsu Y, Chiba A and Fukada E, *Ferroelectrics* **32**:61–67 (1981).
32 Brown TD, Dalton PD and Hutmacher DW, *Adv Mater* **23**:5651–5657 (2011).
33 Gomes J, Serrado Nunes J, Sencadas V and Lanceros-Mendez S, *Smart Mater Struct* **19**:065010 (2010).
34 Lando JB and Doll WW, *J Macromol Sci B* **2**:205–218 (1968).
35 Sencadas V, Gregorio R and Lanceros-Méndez S, *J Macromol Sci B* **48**:514–525 (2009).
36 Liashenko I, Hrynevich A and Dalton PD, *Adv Mater* **32**:2001874 (2020).
37 Uribe-Gomez J, Posada-Murcia A, Shukla A, Ergin M, Constante G, Apsite I *et al.*, *ACS Appl Bio Mater* **4**:1720–1730 (2021).
38 Bakirci E, Schaefer N, Dahri O, Hrynevich A, Strissel P, Strick R *et al.*, *Adv Biosyst* **4**:2000077 (2020).
39 Zhang Q, Xia W, Zhu Z and Zhang Z, *J Appl Polym Sci* **127**:3002–3008 (2013).
40 Schawe JEK, *J Appl Polym Sci* **133**:42977 (2016).
41 Fischer C and Drummer D, *Int J Polym Sci* **2016**:5450708 (2016).
42 Bae J-H and Chang S-H, *Compos Struct* **131**:1090–1098 (2015).
43 Orkwis JA, Wolf AK, Shahid SM, Smith C, Esfandiari L and Harris GM, *Macromol Biosci* **20**:2000197 (2020).
44 Wunner FM, Mieszczanek P, Bas O, Eggert S, Maartens J, Dalton PD *et al.*, *Biofabrication* **11**:025004 (2019).
45 Hrynevich A, Liashenko I and Dalton PD, *Adv Mater Technol* **5**:2000772. (2020).